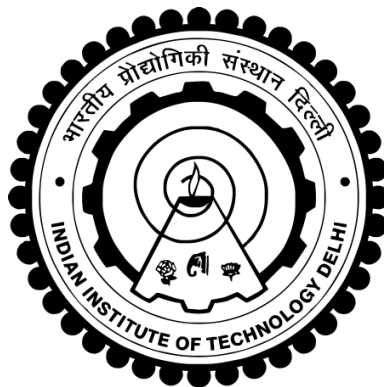


**CONTROL AND IMPLEMENTATION OF SINGLE-PHASE  
GRID INTERFACED SOLAR PV-WIND AND BES BASED  
MICROGRID WITH GRID SYNCHRONIZATION**

**YASHI SINGH**



**DEPARTMENT OF ELECTRICAL ENGINEERING  
INDIAN INSTITUTE OF TECHNOLOGY DELHI  
JUNE 2025**

© Indian Institute of Technology Delhi (IITD), New Delhi, 2025

**CONTROL AND IMPLEMENTATION OF SINGLE-PHASE  
GRID INTERFACED SOLAR PV-WIND AND BES BASED  
MICROGRID WITH GRID SYNCHRONIZATION**

by

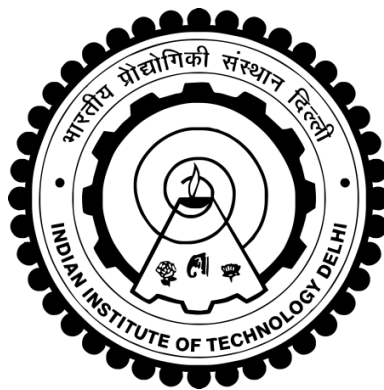
**YASHI SINGH**

**Department of Electrical Engineering**

*Submitted*

*In fulfilment of the requirements of the degree of Doctor of Philosophy*

*to the*



**INDIAN INSTITUTE OF TECHNOLOGY DELHI**

**JUNE 2025**

## **CERTIFICATE**

It is certified that the thesis entitled “**Control and Implementation of Solar-Wind and Battery based Single Phase Microgrid with Grid Synchronization,**” being submitted by Mrs. Yashi Singh for award of the degree of Doctor of Philosophy in the Department of Electrical Engineering, Indian Institute of Technology Delhi, is a record of the student work carried out by her under our supervision and guidance. The matter embodied in this thesis, has not been submitted for the award of any other degree or diploma.

Dated:

**(Prof. Sukumar Mishra)**

**Electrical Engineering Department  
Indian Institute of Technology Delhi  
Hauz Khas, New Delhi-110016, India**

**(Prof. Bhim Singh)**

**Electrical Engineering Department  
Indian Institute of Technology Delhi  
Hauz Khas, New Delhi-110016, India**

## ACKNOWLEDGEMENTS

I am deeply grateful to **Prof. Sukumar Mishra** and **Prof. Bhim Singh** for their invaluable guidance and unwavering support throughout my Ph.D. journey. Working under their mentorship has been a profound experience that has shaped my understanding of research. Prof. Bhim Singh's determination, dedication, innovation, and discipline have been a constant source of inspiration, driving me to push the boundaries of my work and strive for excellence. His consistent encouragement and commitment to my growth have been instrumental in the successful completion of this research.

I extend my sincere thanks to **Prof. Bijaya Ketan Panigrahi**, **Prof. Nilanjan Senroy**, **Prof. G. Bhuvaneshwari**, and **Prof. Ashu Verma**, my SRC members, for their valuable guidance and consistent support. I am also grateful to **Prof. B. K. Panigrahi**, the **late Prof. Mashuq un-Nabi**, **Prof. Indra Narayan Kar**, and **Prof. Anandarup Das** for their foundational contributions during my coursework, which laid the groundwork for my research.

I owe a debt of gratitude to **IIT Delhi** for providing the research facilities that made this work possible. Special thanks to **Prof. G. Bhuvaneshwari**, **Prof. M. Veerachary**, and the staff of the PG Machines Lab., including Mr. Srichand, Mr. Puran Singh, and Mr. Jitendra, for their support during the experimental phases of my work.

I am thankful to my seniors, including Dr. Swati Narula, Dr. Geeta Pathak, Dr. Nidhi Mishra, Dr. Ikhlaiq Hussain, Dr. Nishant Kumar, Dr. Shahdab Murshid, Dr. Shailendra Kumar Dwivedi, Dr. Anjanee kumar Mishra, Dr. Sachin Devassy, Dr. Saurabh Shukla, and Dr. Piyush Kant, for their motivation at the start of my research. I also appreciate the technical and non-technical

support provided by Dr. Ikhlq Hussain, Dr. Aniket Anand, Dr. Radha Kushwaha, Dr. Shailendra Dwivedi, Dr. Anjnee Kumar Mishra, Dr. Anshul Varshney, and Ms. Nupur Saxsena.

I would like to acknowledge Dr. Subrni Pardhan, Ms. Smita Mohanty, and Ms. Farhra Siddique for their constant support and encouragement throughout my Ph.D. work. My gratitude also extends to Dr. Shataskshi Sharma, Dr. Seema, Dr. Vandana Jain, Mrs. Sunaina Singh, Dr. Vineet P. Chandra, Dr. Priyank Shah, Dr. Vivek Narayanan, Dr. Anjeet Verma, Dr. Subhra, Dr. Farheen Chishti, Dr. Pavitra Shukl, and Dr. Tripurari Nath for their encouragement.

I am thankful to my colleagues and friends, including Mr. Gaurav Modi, Mr. Bilal Naqvi, Dr. Sunil Pandey, Dr. Shalvi Tyagi, Dr. Rohini Sharma, Ms. Chandrakala, Ms. Kousalya, Dr. Aryadip Sen, Mr. Sharan Shastri, Dr. Hina Parveen, Mrs. Rashmi Rai, Dr. Suri Paneeth, Dr. Jitendra Gupta, Mr. Rahul Kumar, Mr. Sayandev Ghosh, Mr. Utsav Sharma, Mr. Saran Chaurasiya, Mr. Shivam Yadav, Mr. Deepak Shaw, Mr. Sudip Bhattacharya, Mr. Sandeep Sahoo, Dr. Souvik Das, Ms. Kripa, Mr. Vipin, Mr. Rohit, Mr. Arjun, Mr. Biswajit, Mr. Sumit, and Mr. Himanshu, as well as the entire PG Machines lab group, for their valuable support.

I would also like to express my sincere appreciation to Mr. Yatindra, Mr. Satish, Mr. Sandeep, and all the staff in the Electrical Engineering office for their assistance and cooperation.

On a personal note, I am deeply indebted to my family. I thank my grandfather, Mr. Pritam Singh Verma, my parents, Mrs. Rajni Singh and Mr. Surendra Kumar Singh, my sister, Dr. Shikha Singh, and my aunt Mrs. Sushila Singh for their unwavering support and encouragement.

A special note of thanks goes to my husband, Mr. Veereshwar Pandey. Your steadfast support, patience, and belief in me have been the pillars of my strength throughout this journey. Your

sacrifices and encouragement have been invaluable, and I am forever grateful. To my daughter, Ms. Avya Pandey, your smiles and innocent joy have been my constant source of motivation and inspiration to persevere and complete this thesis.

Finally, I am thankful to the Almighty for the blessings that have guided me to this stage of my academic journey. I pray for continued strength, wisdom, and determination to achieve future goals.

Yashi Singh

## ABSTRACT

This research work focuses on the development of a grid-interactive, multifunctional single-phase PV-BES (Photovoltaic-Battery Energy Storage) system for residential and rooftop applications. To enhance system reliability, configurations integrating battery energy storage (BES) at the DC link are presented, both with and without a bidirectional converter. The functionality of the microgrid in various operating modes is thoroughly discussed. A seamless transition logic, combined with an islanding detection technique, enables smooth transitions between off-grid and grid-interactive modes. In grid-interactive mode, the system effectively provides power quality (PQ) solutions, including harmonics elimination, power factor correction and reactive power compensation. In off-grid mode, the control objectives shift to maintaining voltage and frequency regulation at the point of common coupling (PCC). The primary goal of this system is to ensure uninterrupted power delivery to local critical loads, even during grid outages.

The primary aim of integrating battery energy storage (BES) into the microgrid is to enhance coordination with distributed generation, ensuring a reliable supply of electricity. By integrating BES, the reliability of peak load management is improved, along with the power quality of renewable energy production and the management of distributed and off-grid power systems.

This research work also includes on the development of a grid-interactive multifunctional wind energy generation system (WEGS), objective even during grid outages. Owing to the complementary profiles of renewable sources like wind and solar, this work emphasizes the development of a multifunctional microgrid employing a wind turbine based permanent magnet brushless DC generator (PMBLDCG) and a solar photovoltaic (PV) array. The functionality of the microgrid during various operating modes is discussed. A seamless transition logic, combined with an islanding detection technique, is incorporated for transitioning between off-grid and grid-interactive modes.

This study explores various topologies for parallel solar PV inverter-based microgrids, both with and without BES, aimed at enhancing reliability and accessibility in remote areas. These topologies consist of DG units, BES, and local loads, with each DG unit incorporating inverters connected to a PV array through an output interfacing inductor and coupling lines linked in parallel at the PCC. A microgrid is deemed efficient if it performs effectively in both standalone and grid-tied modes, ensuring a smooth power transition. When a PV inverter operates in

islanding mode, the PV power should not exceed the load demand to maintain system stability. However, this can lead to either wasted PV power or underutilization of available PV power. To address this, additional solar panels are connected to other energy sources, such as batteries, to create a parallel PV inverter-based system, making it feasible to effectively harness power from each source.

The microgrid structures and control algorithms are used in microgrid and these are modelled and simulated with MATLAB/Simulink toolbox. Following satisfactory simulation results, a prototype microgrid incorporating a solar PV array, wind turbine driven PMBLDCG, and BES is developed. Test performances of multiple parallel PV inverter-based microgrids are validated on the RT-LAB platform using a real-time controller OP4510. The simulation and testing results are presented under various challenging conditions, including variations in solar insolation, loads, voltage distortion, and mode transition. Notably, the wind and solar power systems track the maximum power point. Finally, performance of the microgrid in both off-grid and grid-interactive modes, with seamless transitions between these modes, is demonstrated in detail.

## सार

यह शोध कार्य एक ग्रिड-संयुक्त, बहुउद्देशीय एकल-चरणीय सौर-ऊर्जा एवं बैटरी ऊर्जा भंडारण प्रणाली के विकास पर आधारित है, जिसे विशेष रूप से घरेलू एवं छत पर स्थापित अनुप्रयोगों के लिए विकसित किया गया है। प्रणाली की विश्वसनीयता बढ़ाने के उद्देश्य से बैटरी ऊर्जा भंडारण को दिष्ट धारा संधि बिंदु पर एक-दिशीय तथा द्वि-दिशीय परिवर्तकों के साथ तथा बिना संयोजन के विभिन्न विन्यासों में प्रस्तुत किया गया है। इस सूक्ष्मबिजली तंत्र की विभिन्न कार्यप्रणाली स्थितियों में संचालन क्षमता का विस्तृत अध्ययन किया गया है।

एक सुगम संक्रमण युक्ति तथा द्विपीकरण पहचान तकनीक के माध्यम से ग्रिड तथा स्वतंत्र रूप से संचालित मोड के बीच निर्बाध परिवर्तन सुनिश्चित किया गया है। ग्रिड-संयुक्त मोड में यह प्रणाली विद्युत गुणवत्ता सुधार हेतु हार्मोनिक घटाना, शक्ति गुणांक सुधारना तथा प्रत्यावर्ती शक्ति क्षतिपूर्ति जैसे कार्य करती है। स्वतंत्र मोड में प्रणाली का नियंत्रण उद्देश्य संयुक्त युग्मन बिंदु पर वोल्टता एवं आवृत्ति को स्थिर बनाए रखना होता है, जिससे विद्युत आपूर्ति में किसी भी प्रकार की बाधा आने पर भी आवश्यक स्थानीय भारों को सतत ऊर्जा प्राप्त हो सके।

इस प्रणाली में बैटरी ऊर्जा भंडारण को सम्मिलित करने का प्रमुख उद्देश्य है - वितरित ऊर्जा स्रोतों के साथ समन्वय स्थापित करना, ताकि आपूर्ति की विश्वसनीयता सुनिश्चित हो सके। इसके अतिरिक्त यह पीक लोड प्रबंधन, नवीकरणीय ऊर्जा गुणवत्ता तथा दूरवर्ती एवं स्वतंत्र विद्युत तंत्रों के प्रबंधन को भी बेहतर बनाता है।

यह शोध कार्य एक बहुउद्देशीय ग्रिड-संयुक्त पवन ऊर्जा उत्पादन प्रणाली के विकास को भी सम्मिलित करता है। सौर एवं पवन ऊर्जा स्रोतों की पूरक प्रकृति को ध्यान में रखते हुए एक संयुक्त सूक्ष्मबिजली तंत्र विकसित किया गया है, जिसमें स्थायी चुम्बकीय रहित-वलय दिष्ट धारा उत्पादक से चालित पवन टरबाइन एवं सौर ऊर्जा पटल सम्मिलित हैं। इसमें भी सुगम संक्रमण युक्ति तथा द्विपीकरण पहचान तकनीक का प्रयोग किया गया है।

यह अध्ययन बैटरी ऊर्जा भंडारण सहित तथा बिना, समानांतर सौर ऊर्जा इन्वर्टर आधारित सूक्ष्मबिजली तंत्र की विभिन्न संरचनाओं का विश्लेषण करता है, जो दूरदराज़ क्षेत्रों में विद्युत आपूर्ति की उपलब्धता और विश्वसनीयता बढ़ाने में सहायक हैं। इन संरचनाओं में वितरित ऊर्जा इकाइयाँ, ऊर्जा भंडारण प्रणाली और स्थानीय भार शामिल होते हैं, जहाँ प्रत्येक इकाई को सौर पटल, आउटपुट संयोजक और इन्वर्टर के माध्यम से युग्मन बिंदु पर समानांतर रूप में जोड़ा गया है। एक प्रभावशाली सूक्ष्मबिजली तंत्र वही होता है, जो ग्रिड-संयुक्त तथा स्वतंत्र दोनों स्थितियों में कुशलता से कार्य कर सके। स्वतंत्र संचालन के दौरान

यदि सौर ऊर्जा उत्पादन भार की मांग से अधिक हो जाता है, तो प्रणाली की स्थिरता पर प्रभाव पड़ता है। इसे रोकने हेतु अतिरिक्त सौर पटल को ऊर्जा भंडारण तथा अन्य स्रोतों से जोड़ा जाता है, जिससे प्रत्येक स्रोत से प्राप्त ऊर्जा का समुचित उपयोग हो सके।

समस्त सूक्ष्मबिजली संरचनाओं एवं नियंत्रण कलन विधियों को सांख्यिकी गणना सॉफ्टवेयर के माध्यम से मॉडलित एवं अनुकरण किया गया है। संतोषजनक अनुकरण परिणामों के पश्चात एक प्रायोगिक प्रतिरूप तैयार किया गया है, जिसमें सौर पटल, पवन टरबाइन तथा बैटरी ऊर्जा भंडारण को सम्मिलित किया गया है। इस प्रणाली का परीक्षण वास्तविक समय नियंत्रण यंत्र की सहायता से किया गया है। विभिन्न जटिल परिस्थितियों जैसे - सौर विकिरण में परिवर्तन, भार में उतार-चढ़ाव, वोल्टता विकृति एवं संचालन मोड में परिवर्तन की स्थिति में प्राप्त परीक्षण परिणामों का प्रस्तुतीकरण किया गया है। विशेष रूप से सौर एवं पवन दोनों प्रणालियाँ अधिकतम ऊर्जा बिंदु का सफलतापूर्वक अनुसरण करती हैं तथा ग्रिड और स्वतंत्र संचालन मोड के मध्य निर्बाध परिवर्तन को प्रभावी रूप से प्रदर्शित करती हैं।

## TABLE OF CONTENTS

No.		Page
	Certificate	i
	Acknowledgements	ii
	Abstract	v
	Table of Contents	ix
	List of Figures	xix
	List of Tables	xxix
	List of Abbreviations	xxx
	List of Symbols	xxxiii
	<b>CHAPTER I INTRODUCTION</b>	<b>1-7</b>
1.1	General	1
1.2	Microgrids And Standards	1
1.3	Objectives and Scope of Work	5
1.3.1	AC Microgrid with Integrated Solar PV Array	5
1.3.2	AC Microgrid Comprising Wind Energy Conversion System	6
1.3.3	AC Microgrid Comprising Solar PV Array and Wind Energy Conversion System	6
1.3.4	AC Microgrid Comprising Multiple PV Inverters	6
1.4	Organization of Thesis	7
	<b>CHAPTER II LITERATURE REVIEW</b>	<b>10-27</b>
2.1	General	10
2.2	Development and Standards in Microgrids	11

2.3	Literature Survey	11
2.3.1	Review on Solar Energy Generation System (SEGS)	12
2.3.2	Review of Maximum Power Extraction (MPE) Techniques for Solar Energy Generation System	15
2.3.3	Review on Wind Energy Conversion System (WECS)	15
2.3.4	Review of MPE for WECS	18
2.3.5	Review of Energy Storage System Technologies in Microgrid	18
2.3.6	Review of Hybrid Renewable Energy based Microgrid	19
2.3.7	Review on AC Microgrid Comprising Multiple Solar PV Array	20
2.2.8	Review of Islanding Detection and Synchronization Techniques Used in Microgrid	22
2.2.9	Power Quality Issues and Mitigation Techniques in Grid-Interactive Microgrids	24
2.3	Identified Research Areas	26
2.4	Conclusions	27
<b>CHAPTER III</b>	<b>CONTROL AND IMPLEMENTATION OF SINGLE-PHASE SOLAR PV BASED MICROGRID WITH GRID SYNCHRONIZATION</b>	28-107
3.1	General	28
3.2	Configurations of Single-Phase Grid Interactive Solar PV Based Microgrid	28
3.2.1	Single-Stage Solar PV-based Microgrid with Bidirectional Converter Controlled BES	28
3.2.2	Two Stage Solar PV Microgrid with BES on DC Link	29
3.2.3	Two-Stage Solar PV based Microgrid with Bidirectional Converter Controlled BES	30
3.3	Design of Single-Phase Grid Interactive Solar PV Based Microgrids	32
3.3.1	Design and Selection of Solar PV array	33
3.3.2	Design and Selection of DC Bus Voltage	33
3.3.3	Design and Selection of DC Bus Capacitor	34
3.3.4	Design and Selection of Interfacing Inductors	34

3.3.5	Design and Selection of Ripple Filter	34
3.3.6	Design and Selection of Battery Energy Storage	35
3.3.7	Design and Selection of Boost Converter	35
3.3.8	Design of Inductor for Bidirectional Converter (DBC)	36
3.3.9	Design and Selection of VSC Switching devices	36
3.4	Control Approaches of Solar PV-based Microgrid with Grid Synchronization	37
3.4.1	Control Approach of Single Stage Solar Microgrid with Bidirectional Buck-boost Converter Controlled BES	38
3.4.1.1	MPE Control for Solar PV array	38
3.4.1.2	Control Approach for DC-DC Bidirectional Converter	39
3.4.1.3	Control Approach for VSC for Grid Tide Mode of Operation	41
3.4.1.4	Control Approach for VSC for Islanding Mode of Operation	46
3.4.1.2	Control of Mode Transition Logic	46
3.4.2	Control Approach of Two Stage PV Based Microgrid with BES on DC Link	47
3.4.2.1	MPE from Solar PV Array	48
3.4.2.2	Control Approach for VSC for Grid Tide Mode of Operation	51
3.4.2.3	Control Approach for VSC for Islanding Mode of Operation	54
3.4.2.4	Control of Transition Logic	55
3.4.3	Control Approach of Two Stage Solar Microgrid with Bidirectional Buck-boost Converter Controlled BES	57
3.4.3.1	MPE from Solar PV Array	
3.4.3.2	Control Approach for DC-DC Bidirectional Converter	58
3.4.3.3	Control Approach for VSC for Grid Tide Mode of operation	61
3.4.3.4	Control Approach for VSC for Islanding Mode of Operation	65
3.4.3.6	Control of Mode Transition Logic	66
3.5	MATLAB based Modeling of Single-Phase Grid Interactive PV Based Microgrids	67

3.5.1	MATLAB based Modeling of Single Stage Solar Microgrid with Bidirectional Converter Controlled BES	68
3.5.2	MATLAB based Modeling of Two Stage Solar Microgrid with BES on DC Link	68
3.5.3	MATLAB based Modeling of Two Stage Solar Microgrid with Bidirectional Buck-boost Converter Controlled BES	69
3.6	Hardware Implementation of Single-Phase Grid Interactive PV Based Microgrids	69
3.6.1	Development of Solar Array Using Simulator	70
3.6.2	Hardware Configuration of DSP d-SPACE-1202 Controller	70
3.6.3	Interfacing Circuit for Hall Effect Current Sensors	71
3.6.4	Interfacing Circuit for Hall Effect Voltage Sensors	72
3.6.5	Interfacing Circuit for Gate Driver	73
3.7	Results and Discussion	74
3.7.1	Performance of Two Stage PV Based Microgrid with BES on DC Link	75
3.7.1.1	Simulated Performance	75
3.7.1.2	Experimental Performance	80
3.7.2	Performance of Single Stage PV Based Microgrid with Bidirectional Converter Controlled BES	86
3.7.2.1	Simulated Performance	86
3.7.2.2	Experimental Performance	90
3.7.3	Performance of Two Stage PV Based Microgrid with Bidirectional Converter Controlled BES	95
3.7.3.1	Simulated Performance	96
3.7.3.2	Experimental Performance	100
3.8	Conclusions	107
<b>CHAPTER IV</b>	<b>CONTROL AND IMPLEMENTATION OF SINGLE-PHASE WIND-BASED MICROGRID WITH GRID SYNCHRONIZATION</b>	108-154
4.1	General	108
4.2	Configurations of Single-Phase Grid Interactive Wind-Based Microgrids	108

4.2.1	Microgrid Employing Two Stage Wind with BES on DC Link	108
4.2.2	Microgrid Employing Two-Stage Wind-based Bidirectional Converter Controlled BES	109
4.3	Design of Single-Phase Grid Interactive Wind-Based Microgrids	110
4.3.1	Design and Selection of Wind Turbine	111
4.3.2	Modelling of Wind Turbine	111
4.2.3	Modelling of PMBLDCG	114
4.4	Control Approach of Single-Phase Grid Interactive Wind-Based Microgrids	114
4.4.1	Control Approach of Two-Stage Wind Microgrid with BES on DC Link	117
4.4.1.1	MPE from Wind turbine	117
4.4.1.2	Control Approach for VSC for Grid Tide Mode of Operation	119
4.4.1.3	Control Approach for VSC for Islanding Mode of Operation	122
4.4.1.4	Control of Mode Transition Logic	122
4.4.2	Control Approach of Two-Stage Wind-based Microgrid with Bidirectional Buck-boost Converter Controlled BES	124
4.4.2.1	MPE from Wind turbine	124
4.4.2.2	Control Approach for Bidirectional Converter	126
4.4.2.3	Control Approach for VSC for Grid Tide Mode of Operation	126
4.4.2.4	Control Approach for VSC for Islanding Mode of Operation	128
4.4.2.5	Control of Mode Transition Logic	128
4.5	MATLAB-based Modeling of Single-Phase Grid Interactive PV Based Microgrids	130
4.5.1	MATLAB-based Modeling of Two-Stage Wind Microgrid with BES on DC Link	130
4.5.2	MATLAB-based Modeling of a Two-Stage Wind-based Microgrid with Bidirectional Buck-boost Converter Controlled BES	131
4.6	Hardware Implementation of Single-Phase Grid Interactive-Based Microgrids	131
4.7	Results and Discussion	134

4.7.1	Performance of Two-Stage Wind Microgrid with BES on DC Link	134
4.7.1.1	Simulated Performance	134
4.7.1.2	Experimental Performance	137
4.7.2	Performance of Two-Stage Wind-based Microgrid with Bidirectional Buck-boost Converter Controlled BES	141
4.7.2.1	Simulated Performance	141
4.7.2.2	Experimental Performance	147
4.8	Conclusions	154
<b>CHAPTER V</b>	<b>CONTROL AND IMPLEMENTATION OF SINGLE-PHASE SOLAR PV AND WIND-BASED MICROGRID WITH GRID SYNCHRONIZATION</b>	155-207
5.1	General	155
5.2	Configurations of Single-Phase Grid Interactive PV and Wind-Based Microgrids	155
5.2.1	Single-Phase Single-Stage PV-Wind Microgrid with Bidirectional Buck-boost Converter Controlled BES	155
5.2.2	Single-Phase Two-Stage PV-Wind Microgrid with BES on DC Link	156
5.2.3	Single-Phase Two-Stage PV-Wind Microgrid with Bidirectional Buck-boost Converter Controlled BES	158
5.3	Design of Single-Phase Grid Interactive PV and Wind-Based Microgrids	159
5.3.1	Design and Selection of Solar Photovoltaic Array	159
5.3.2	Design and Selection of DC link Capacitor	159
5.3.3	Design and Selection of Inductor of Boost Converter for Solar PV array	159
5.3.4	Design and Selection of Battery Energy Storage	159
5.3.5	Design and Selection of Bidirectional Converter	161
5.3.6	Design and Selection of Wind Turbine	161
5.3.7	Design and Selection of Inductor of Boost Converter for Wind Energy	161
5.4	Control of Single-Phase PV-Wind Microgrid with BES	161
5.4.1	Control of Single-Phase Single-Stage PV-Wind Microgrid with Bidirectional Buck-boost Converter Controlled BES	163

5.4.1.1	MPE from Solar PV Array	163
5.4.1.2	MPE from Wind Turbine	163
5.4.1.3	Control Structure for Bidirectional Converter	164
5.4.1.4	Control Approach for VSC for Grid Tide Mode of Operation	164
5.4.1.4	Control Approach for VSC for Islanding Mode of Operation	168
5.4.1.5	Control of Mode Transition Logic	168
5.4.2	Control of Single-Phase Two-Stage PV-Wind Microgrid with BES on DC Link	169
5.4.2.1	MPE from Solar PV Array	170
5.4.2.2	MPE from Wind turbine	170
5.4.2.3	Control Approach for VSC for Grid Tide Mode of Operation	171
5.4.2.4	Control Approach for VSC for Islanding Mode of Operation	173
5.4.2.5	Control of Mode Transition Logic	173
5.4.5	Control Approach of Single-Phase Two-Stage PV-Wind Microgrid with Bidirectional Buck-boost Converter Controlled BES	174
5.4.5.1	MPE from Solar PV Array	175
5.4.5.2	MPE from Wind turbine	175
5.4.5.3	Control Structure for Bidirectional Converter	175
5.4.5.4	Control Approach for VSC for Grid Tide Mode of Operation	176
5.4.5.5	Control Approach for VSC for Islanding Mode of Operation	178
5.4.5.6	Control of Mode Transition Logic	178
5.5	MATLAB based Modeling of Single-Phase Grid Interactive PV-Wind Based Microgrids	180
5.5.3	MATLAB based Modeling of Single Stage Solar-Wind Microgrid with Bidirectional Buck-boost Converter Controlled BES	180
5.5.4	MATLAB based Modeling of Single-Phase Two-Stage PV-Wind Microgrid with BES on DC Link	180

5.5.5	MATLAB based Modeling of Single-Phase Two-Stage PV-Wind Microgrid with Bidirectional Buck-boost Converter Controlled BES	182
5.6	Hardware Implementation of Single-Phase Grid Interactive PV-Wind-Based Microgrids	182
5.7	Results and Discussion	184
5.7.1	Performance of Single Stage Solar-Wind Microgrid with BES on DC Link with Bidirectional Buck-boost Converter Controlled BES	184
5.7.1.1	Simulated Performance	185
5.7.1.2	Experimental Performance	188
5.7.2	Performance of Single-Phase Two-Stage PV-Wind Microgrid with BES on DC Link	191
5.7.2.1	Simulated Performance	193
5.7.2.2	Experimental Performance	196
5.7.3	Performance of Single-Phase Two-Stage PV-Wind Microgrid with Bidirectional Buck-boost Converter Controlled BES	200
5.7.3.1	Simulated Performance	200
5.7.3.2	Experimental Performance	203
5.8	Conclusions	207
<b>CHAPTER VI</b>	<b>CONTROL AND IMPLEMENTATION OF SINGLE PHASE MULTIPLE PARALLEL SOLAR PV INVERTER-BASED MICROGRIDS</b>	<b>208-240</b>
6.1	General	208
6.2	Configurations of Multiple Parallel PV Inverter-Based Microgrids	209
6.2.1	Single-Phase Single-Stage Multiple Parallel PV Inverter-Based Microgrid	209
6.2.2	Single-Phase Two-Stage Multiple Parallel PV Inverter-Based Microgrid	209
6.3	Design of Single-Phase Multiple Parallel PV Inverter-Based Microgrids	211
6.4	Control Approach of Single-Phase Multiple Parallel PV Inverter-Based Microgrids	212
6.4.1	Control Approach of Single-Phase Single-Stage Multiple Parallel PV Inverter-Based Microgrid	213
6.4.1.1	MPE Control	214

6.3.1.2	Control Approach of VSCs	214
6.3.1.2	Control of Mode transition Logics	218
6.4.2	Control Approach of Single-Phase Two-Stage Multiple Parallel PV Inverter-Based Microgrid Without BES	219
6.4.2.1	MPE Control	219
6.4.2.2	Control Approach of VSCs	220
6.4.2.3	Control of Mode transition Logics	223
6.5	MATLAB Modeling of Single-Phase Single-Stage Multiple Parallel PV Inverter-Based Microgrids Without BES	224
6.5.1	Simulation Model of Single-Phase Single-Stage Multiple Parallel PV Inverter-Based Microgrid	225
6.5.2	Simulation Model of Single-Phase Two-Stage Multiple Parallel PV Inverter-Based Microgrid	225
6.6	Real Time Testing of Single-Phase Single-Stage Multiple Parallel PV Inverter-Based Microgrids	226
6.7	Results and Discussion	227
6.7.1	Performance of Single-Phase Single-Stage Multiple Parallel PV Inverter-Based Microgrid	227
6.7.1.1	Simulated Performance	227
6.7.1.2	Test Performance	230
6.7.1.2	Performance of Single-Phase Two-Stage Multiple Parallel PV Inverter-Based Microgrid	233
6.7.2.1	Simulated Performance	234
6.7.2.2	Test Performance	234
6.8	Conclusion	239
<b>CHAPTER VII</b>	<b>CONTROL AND IMPLEMENTATION OF SINGLE PHASE MULTIPLE PARALLEL SOLAR PV-BES INVERTER BASED MICROGRIDS</b>	<b>241-289</b>
7.1	Introduction	241
7.2	Configurations and Objectives of Multiple Parallel Solar PV-BES Inverter Based Microgrids	242
7.2.1	Single-Stage Multiple Parallel Solar PV Inverter Based Microgrid with Bidirectional Converter Controlled BES	242
7.2.2	Single-Phase Single-Stage Multiple Parallel Solar PV Inverter Based Microgrid with BES on DC Link	234
7.2.3	Single-Phase Two-Stage Multiple Parallel Solar PV Inverter Based Microgrid with Bidirectional Converter Controlled BES	244

7.3	Design of Single-Phase Multiple Parallel Solar PV-BES Inverter Based Microgrids	245
7.4	Control Approach of Single-Phase Multiple Parallel Solar PV-BES Inverter-Based Microgrids	246
7.4.1	Control Approach of Single-Stage Multiple Parallel Solar PV Inverter Based Microgrid with Bidirectional Converter Controlled BES	249
7.4.1.1	MPE Control	249
7.4.1.2	Control Approach of VSCs	249
7.4.1.3	Control of Mode transition Logics	254
7.4.2	Control Approach of Single-Phase Single-Stage Multiple Parallel Solar PV Inverter-Based Microgrid with BES on DC Link	255
7.4.2.1	MPE Control	256
7.4.2.2	Control Approach of VSCs	256
7.4.2.3	Control of Mode transition Logics	260
7.4.3	Control Approach of Single-Phase Two-Stage Multiple Parallel Solar PV Inverter-Based Microgrid with Bidirectional Converter Controlled BES	261
7.4.3.1	MPE Control	262
7.4.3.2	Control Approach of VSCs	262
7.4.3.3	Control of Mode transition Logics	266
7.5	MATLAB Modeling of Single-Phase Single-Stage Multiple Parallel Solar PV-BES Inverter Based Microgrids	267
7.5.1	Simulation Model of Single-Stage Multiple Parallel Solar PV Inverter Based Microgrid with Bidirectional Converter Controlled BES	267
7.5.2	Simulation Model of Single-Phase Single-Stage Multiple Parallel Solar PV Inverter-Based Microgrid with BES on DC Link	267
7.5.3	Simulation Model of Single-Phase Two-Stage Multiple Parallel PV Inverter-Based Microgrid with Bidirectional Converter Controlled BES	268
7.6	Real Time Implementation of Single-Phase Single-Stage Multiple Parallel Solar PV-BES Inverter-Based Microgrids	269
7.7	Results and Discussion	270
7.7.1	Performance of Single-Stage Multiple Parallel Solar PV Inverter Based Microgrid with Bidirectional Converter Controlled BES	271

7.7.1.1	Simulated Performance	271
7.7.1.2	Test Performance	271
7.7.2	Performance of Single-Phase Single-Stage Multiple Parallel Solar PV Inverter-Based Microgrid with BES on DC Link	276
7.7.2.1	Simulated Performance	276
7.7.2.2	Test Performance	277
7.7.3	Performance of Single-Phase Two-Stage Multiple Parallel PV Inverter Based Microgrid with Bidirectional Converter Controlled BES	282
7.7.3.1	Simulated Performance	283
7.7.3.2	Test Performance	286
7.8	Conclusions	289
<b>CHAPTER VIII</b>	<b>MAIN CONCLUSIONS AND SUGGESTIONS FOR FURTHER WORK</b>	290-292
8.1	General	290
8.2	Main Conclusions	291
8.3	Suggestions for Further Work	292
	<b>REFERENCES</b>	294
	<b>LIST OF PUBLICATIONS</b>	314
	<b>BIO-DATA</b>	317

## LIST OF FIGURES

- Fig. 3.1 Single-stage solar and bidirectional buck-boost converter-controlled BES based microgrid with grid synchronization.
- Fig. 3.2 Single stage solar based microgrid with grid synchronization
- Fig. 3.3 Two-stage solar and bidirectional converter-controlled BES based microgrid with grid synchronization.
- Fig. 3.4 Control scheme of single stage PV-based microgrid.
- Fig. 3.5 P&O algorithm
- Fig. 3.6 Equivalent circuit model of the DBC
- Fig. 3.7 Bode plot of the voltage and current control of the DBC
- Fig. 3.8 Frequency response of MOGI in comparison to SOGI, SO-SOGI and TOGI
- Fig. 3.9 Pole-zero plot of MOGI
- Fig. 3.10 Mode transition control for mode shifting
- Fig. 3.11 Control algorithm of single-phase PV-BES based microgrid
- Fig. 3.12 Equivalent model of boost converter interfaced with solar PV array
- Fig. 3.13 Bode plot of the boost converter and the designed controller
- Fig. 3.14 Bode plots of AQSG technique (a) in-phase component (b) quadrature component.
- Fig. 3.15 Mode transition algorithm
- Fig. 3.16 Mode transition logic
- Fig. 3.17 Control scheme of two stage PV based microgrid (a) grid current control, (b) NMSOGI-PLL, and (c) voltage control
- Fig. 3.18 Equivalent circuit model of bidirectional converter
- Fig. 3.19 (a) DBC Control Loop (b) Bode Plot of  $I_b$  and  $V_{dc}$  TF (c) Bode Plot of current loop and voltage control
- Fig. 3.20 Structure of modified novel sinusoidal second order quadrature signal generator
- Fig. 3.21 Bode Plot of  $H_d(s)$  and  $H_q(s)$
- Fig. 3.22 Flowchart diagram of the system in different modes of operation
- Fig. 3.23 Block diagram of mode transition logic
- Fig. 3.24 Mode transition control for mode shifting.
- Fig. 3.25 MATLAB model of the PV interfaced AC microgrid
- Fig. 3.26 MATLAB model of the PV interfaced AC microgrid
- Fig. 3.27 MATLAB model of the two-stage solar microgrid with DBC controlled BES

- Fig. 3.28 Developed prototype (1) PV Array Simulator PC, (2) solar PV array simulator, (3) DSO (4) simulator PC (5) Voltage and current sensors (6) opto-couplers, (7) current probe, (8) power analyses (9) auto-transformer, (10) voltage source converter, (11) bidirectional converter, (12) power supply, (13) inductor (14) interfacing inductors, (15) controller dSPACE Microlab box 1202, (16) loads, (17) lead acid battery and (18) diode bridge rectifier
- Fig. 3.29 Photograph of dSPACE MicroLabBox DS1202
- Fig. 3.30 Current sensing circuitry (a) schematic diagram and (b) developed hardware prototype.
- Fig. 3.31 Voltage sensing circuitry (a) schematic diagram and (b) developed hardware prototype
- Fig. 3.32 Opto-isolation circuitry (a) schematic diagram and (b) developed hardware prototype
- Fig. 3.33 Performance of a single stage microgrid under the solar insolation variation
- Fig. 3.34 Simulation performance of a single stage microgrid under load variation
- Fig. 3.35 Simulation performance of a single stage microgrid under mode transition
- Fig. 3.36 Harmonic spectra of single stage AC microgrid (a) grid voltage, (b) grid current, (c) load current, and (d) PCC voltage
- Fig. 3.37 Performance of the system under constant grid power (a)  $v_g$ ,  $i_g$  (b) grid power ( $P_g$ ) (c) harmonic spectrum of  $i_g$  (d) harmonic spectrum of  $v_g$  (e)  $v_L$ ,  $i_L$  (f) load power ( $P_L$ ) (g) harmonic spectrum of  $v_g$  (h)  $v_c$ ,  $i_c$  (i) converter power ( $P_c$ ) (j)  $V_{pv}$ ,  $I_{pv}$ , (k) PV power ( $P_{pv}$ ), and (l)  $V_b$ ,  $I_b$
- Fig. 3.38 System performance during the change in solar irradiation from 1000 W/m<sup>2</sup> to 700 W/m<sup>2</sup> (a)  $V_{pv}$ ,  $I_{pv}$ ,  $V_b$ ,  $I_b$  (b)  $V_{dc}$ ,  $i_g$ ,  $i_L$ ,  $I_{pv}$  from 700 W/m<sup>2</sup> to 1000 W/m<sup>2</sup> (c)  $V_{pv}$ ,  $I_{pv}$ ,  $V_b$ ,  $I_b$  (d)  $V_{dc}$ ,  $i_g$ ,  $i_L$ ,  $I_{pv}$ , Solar PV array characteristics at (e) 700 W/m<sup>2</sup> (f) 1000 W/m<sup>2</sup>
- Fig. 3.39 System performance in IAM under varying load
- Fig. 3.40 System response under IAM (a)  $V_L$ ,  $I_L$  (b)  $P_L$  (c) Harmonic spectrum of  $v_L$  (d)  $V_{PV}$  and  $I_{PV}$ , (e)  $I_b$  and  $V_b$ , and (f)  $P_b$
- Fig. 3.41 Dynamic performance of PV based microgrid for grid disconnection
- Fig. 3.42 Dynamic performance of the system during grid reconnection (a)  $v_g$ ,  $i_g$ ,  $v_L$ ,  $i_L$  (b)  $i_L$ ,  $\theta_g$ ,  $\theta_L$ ,  $i_g$
- Fig. 3.43 Fig. 3.43 System dynamic performance (a) PV-VSC mode to APF mode (b) APF mode to PV-VSC mode
- Fig. 3.44 Response of a grid tied to two stage PV microgrid under variable solar insolation.
- Fig. 3.45 Fig. 3.45 Performance of a two stage AC microgrid under mode transition
- Fig. 3.46 Harmonic spectra of single stage AC microgrid (a)  $v_g$ , (b)  $i_g$ , (c)  $v_L$  and (c)  $i_L$

- Fig. 3.47 System response while feeding constant grid power (a)  $v_g, i_g$  (b) grid power ( $P_g$ ) (c) harmonic spectrum of  $v_g$  (d) harmonic spectrum of  $i_g$  (e)  $v_L, i_L$  (f) load power ( $P_L$ ) (g)  $v_c, i_c$  (h) converter power ( $P_c$ ) (i)  $V_{pv}, I_{pv}$  (j) PV power (k)  $V_b, I_b$  (l) battery power ( $P_b$ )
- Fig. 3.48 System response during changes in insolation from 1000 W/m<sup>2</sup> to 700 W/m<sup>2</sup> (a)  $V_{pv}, I_{pv}, V_b, I_b$  (b)  $v_g, i_g, i_L, I_{pv}$  Solar PV array characteristics at (c) 700 W/m<sup>2</sup> (d) 1000 W/m<sup>2</sup>
- Fig. 3.49 Dynamic response of the microgrid in response to a decreasing load.
- Fig. 3.50 System response in IAM (a)  $V_L, I_L$  (b)  $P_L$  (c-d) Harmonic spectrum of  $v_L$  and  $i_L$  (e)  $V_b, I_b$  (f)  $P_b$  (g)  $V_{pv}, I_{pv}$  (h)  $P_{pv}$
- Fig. 3.51 (a-b) Test performance of a two stage PV-BES-based microgrid under mode transition from GTM to IAM and vice-versa
- Fig. 3.52 Dynamic performance of two stage PV-BES system under during PV hour
- Fig. 3.53 Response of microgrid under mode transition
- Fig. 3.54 Simulated performance of the MNSOGI-PLL under the grid distorted condition
- Fig. 3.55 System response while supplying constant power to the grid (a)  $v_g, i_g$  (b) grid power ( $P_g$ ) (c) harmonic spectrum of  $v_g$  (d) harmonic spectrum of  $i_g$  (e)  $v_L, i_L$  (f) load power ( $P_L$ ) (g) harmonic spectrum of  $i_L$  (h)  $v_c, i_c$  (i) converter power ( $P_c$ ) (j)  $V_b, I_b$  (k)  $V_{PV}, I_{PV}$  (l) PV power ( $P_{PV}$ )
- Fig. 3.56 Dynamic response of the system under change of solar irradiation (a)  $v_g, V_{dc}, i_g, I_{PV}$  (b)  $V_{dc}, i_L, I_b, i_c$
- Fig. 3.57 Dynamic response of the system under load change a)  $V_{PV}, i_L, I_b, i_c$  (b)  $v_g, V_{dc}, i_g, I_{PV}$  and (c)  $P_g, P_L, P_{PV}$  and  $I_{PV}$
- Fig. 3.58 Dynamic response of system under mode change (a)  $i_g, I_{PV}, i_L, P_{PV}$  (b)  $v_g, V_{dc}, i_g, i_c$  and (c)  $I_{PVFF}, I_{PL}, I_{Loss}$  and  $I_{gref}$
- Fig. 3.59 System response in IAM (a)  $V_L, I_L$  (b)  $P_L$  (c-d) Harmonic spectrum of  $v_L$  and  $i_L$  (e)  $V_{pv}, I_{pv}$  (f)  $P_{pv}$  (g)  $V_b, I_b$  (h)  $P_b$
- Fig. 3.60 Test responses of two-stage PV-BES based microgrid under mode transition
- Fig. 3.61 Test responses of two-stage PV-BES based microgrid under mode transition.
- Fig. 4.1 Two-stage wind and BES-based microgrid with grid synchronization.
- Fig. 4.2 Configuration of two-stage wind-based microgrid with bidirectional buck-boost converter-controlled BES
- Fig. 4.3 Equivalent circuit of PMBLDCG
- Fig. 4.4 Wind turbine power vs wind turbine speed
- Fig. 4.5 Control scheme of two-stage wind microgrid with BES on DC link
- Fig. 4.6 P&O-based control algorithm for wind power extraction
- Fig. 4.7 Control structure of boost converter control.
- Fig. 4.8 Structure of GE-EPLL

- Fig. 4.9. Mode transition control for mode shifting.
- Fig. 4.10 Control scheme of two-stage wind-based microgrid with bidirectional buck-boost converter-controlled BES
- Fig. 4.11 Maximum power extraction control for wind turbine
- Fig. 4.12 Block diagram of seamless transition logic for mode shifting.
- Fig. 4.13 MATLAB model of a grid-interactive WEGS-based microgrid
- Fig. 4.14 Two-stage wind microgrid with bidirectional converter-controlled BES
- Fig. 4.15 Photograph of developed prototype in the laboratory
- Fig. 4.16 Simulation performance of a wind-BES-based microgrid under mode transition
- Fig. 4.17 Simulation performance of a wind-BES-based microgrid under mode transition
- Fig. 4.18 Harmonic spectra of wind-BES-based microgrid (a) grid voltage, (b) grid current, (c) load current, and (d) VSC current
- Fig. 4.19 Wind-BES microgrid at utility-integrated mode (a) wind current and wind voltage, (b) PCC voltage and load current, (c) grid voltage and grid current, (d) BES current and BES voltage, (e) load power, (f) VSC power, (g) harmonic spectra of grid voltage, (h) harmonic spectra of load current, and (i) harmonic spectra of grid current.
- Fig. 4.20 Test results of wind-BES microgrid in islanding mode (IAM) (a) wind voltage and wind current, (b) wind power, (c) load current and voltage, (d) load power, (e) BES voltage and BES current, (f) BES power, (g) harmonic spectra of load current, and (h) harmonic spectra of PCC voltage.
- Fig. 4.21 Test results of a wind-BES-based microgrid during load variation
- Fig. 4.22 Test results of microgrid employing wind and BES under wind speed variation.
- Fig. 4.23 Test results of AC microgrid employing wind-BES under mode transition.
- Fig. 4.24 Simulation performance of a wind-BES-based microgrid under mode transition
- Fig. 4.25 Performance of a two stage AC microgrid under load variation
- Fig. 4.26 Performance of an AC microgrid under the presence of grid distortion
- Fig. 4.27 Harmonic spectra of wind-BES-based microgrid (a) grid voltage, (b) grid current, (c) load current, and (d) VSC current
- Fig. 4.28 Test results of wind-BES based grid tied system (a) wind voltage and wind current, (b) wind power, (c) load current and voltage, (d) load power, (e) BES voltage and BES current, (f) BES power, (g) harmonic spectra of load current, and (h) harmonic spectra of PCC voltage.

- Fig. 4.29 Test results of AC microgrid in islanding mode (a)  $i_{wa}$  and  $v_{wa}$ , (b) wind power, (c) load current and voltage, (d) load power, (e)  $V_b$  and  $I_b$ , (f) BES power, (g) harmonic spectra of load current, and (h) harmonic spectra of PCC voltage.
- Fig. 4.30 Test performance of AC microgrid with DBC controlled BES under wind speed variation
- Fig. 4.31 Test results of a wind-based microgrid with bidirectional converter-controlled BES under the wind power variation
- Fig. 4.32 Test results of AC microgrid with DBC controlled BES under the mode transition
- Fig. 5.1 Single-stage solar-wind and bidirectional buck-boost converter-controlled BES-based microgrid with grid synchronization.
- Fig. 5.2 Single stage solar and wind based microgrid with grid synchronization.
- Fig. 5.3 Two-stage solar and bidirectional buck-boost converter-controlled BES based microgrid with grid synchronization
- Fig. 5.4 Control scheme of single stage hybrid AC microgrid (a) VSC control, (b) standalone voltage control, (c) estimation of grid voltage amplitude and unit template and (d) structure of MADO.
- Fig. 5.5 Bode plot of adaptive circular noise estimation observer.
- Fig. 5.6 Block diagram of mode transition logic
- Fig. 5.7 Control scheme of two stage hybrid microgrid (a) VSC switching scheme, (b) standalone voltage control, (c) estimation of grid voltage amplitude and unit template and (d) structure of ANI.
- Fig. 5.8 Block diagram of mode transition logic.
- Fig. 5.9 Control scheme of PV wind and BES based microgrid (a) VSC control, (b) standalone voltage control, (c) estimation of grid voltage amplitude and unit template and (d) structure of MCVF
- Fig. 5.10 Block diagram of seamless transition logic for mode shifting.
- Fig. 5.11 MATLAB model of a single-stage hybrid microgrid
- Fig. 5.12 MATLAB model of a two-stage hybrid microgrid
- Fig. 5.13 MATLAB model of a two-stage hybrid microgrid
- Fig. 5.14 Developed prototype of developed PV-wind and BES based microgrids
- Fig. 5.15 MATLAB model of a two-stage hybrid microgrid
- Fig. 5.16 Harmonic spectra of single stage hybrid AC microgrid (a)  $v_g$ , (b)  $i_g$ , (c)  $v_L$  and (c)  $i_L$
- Fig. 5.17 Test results of PV wind-BES based grid-tied system voltage (a)  $I_{PV}$  and  $V_{PV}$  (b)  $i_{wa}$  and  $v_{wa}$ , (c) wind power, (d)  $i_g$  and  $v_g$ , (e) grid power, (f)  $i_c$  and  $v_c$ , (g) VSC power, (h) load current and voltage (i) load power, (j)  $I_b$  and  $V_b$  (k) harmonic spectra of  $i_g$  and (h) harmonic spectra of  $v_g$

- Fig. 5.18 Test results of wind-BES microgrid in islanding mode (a)  $v_{wa}$  and  $i_{wa}$ , (b) wind power, (c)  $i_L$  and  $v_L$ , (d) load power, (e)  $V_b$  and  $I_b$ , (f) BES power, (g) harmonic spectra of  $i_L$ , and (h) harmonic spectra of  $v_g$
- Fig. 5.19 Performance of single stage microgrid under the RES power variation
- Fig. 5.20 Performance of single stage microgrid under the load variation at PCC
- Fig. 5.21 Mode transition performance of single stage PV wind and BES based system
- Fig. 5.22 Performance of a hybrid AC microgrid under mode transition
- Fig. 5.23 Harmonic spectra of single stage hybrid AC microgrid (a) grid voltage, (b) grid current, (c) PCC voltage and (c) load current
- Fig. 5.24 Test results of PV wind-BES based grid-tied system voltage (a) PV current and voltage (b) wind current and voltage, (c) wind power, (d) grid power, (e) grid current and voltage, (f) VSC voltage and current, (g) VSC power, (h) load current and voltage (i) BES current and voltage, (j) harmonic spectra of load current (k) harmonic spectra of grid current and (h) harmonic spectra of grid voltage
- Fig. 5.25 Test results of wind-BES microgrid in islanding mode (a) wind voltage and wind current, (b) wind power, (c) load current and voltage, (d) load power, (e) BES voltage and BES current, (f) BES power, (g) harmonic spectra of load current, and (h) harmonic spectra of PCC voltage.
- Fig. 5.26 Performance of double stage microgrid under the RES power variation
- Fig. 5.27 Mode transition performance of two stage PV wind and BES based system
- Fig. 5.28 Mode transition performance of two stage PV wind and BES based system
- Fig. 5.29 (a) Simulated Performance of the microgrid under the distortion, (c-d) Simulated performance of control algorithms in the presence of DC offset error, (b) MACNE algorithm, (c) SOGI-FLL, (d) TOGI and (e) FADO and (f) Lissajous pattern of MCVF
- Fig. 5.30 Test results of PV wind-BES based grid-tied system voltage (a) IPV and VPV (b)  $i_{wa}$  and  $v_{wa}$ , (c) wind power, (d)  $i_g$  and  $v_g$ , (e) grid power, (f)  $i_c$  and  $v_g$ , (g) VSC power, (h)  $i_L$  and  $v_L$  (i) load power, (j)  $I_b$  and  $V_b$  (k) harmonic spectra of  $i_g$  and (h) harmonic spectra of  $v_g$
- Fig. 5.31 Test results of wind-BES microgrid in islanding mode (a) (b) PV voltage and PV current, (b) PV voltage and PV current, (c) load current and voltage, (d) load power, (e) harmonic spectra of load current, (f) harmonic spectra of PCC voltage, (g) BES voltage and BES current and (h) BES power,
- Fig. 5.32 Performance of two stage microgrid at variable power generation from RESs
- Fig. 5.33 Fig. 5.34 Performance of two stage microgrid under the load injection
- Fig. 5.34 Mode transition performance of two stage PV wind and BES based system.
- Fig. 6.1 Single Stage multiple parallel PV inverter-based microgrid
- Fig. 6.2 Single phase two stage multiple parallel PV inverter-based microgrid

- Fig. 6.3 Control scheme of PVI-1 (a) grid current control, (b) islanding control, (c-d) N-GI PLL and (e) N-GI structure
- Fig. 6.4 Control scheme of PVI-2
- Fig. 6.5 (a) PLL and (b) mode transition control (MTC)
- Fig. 6.6 Boost converter switching logic for MPE
- Fig. 6.7 Control scheme of PVI-1 (a) grid current control, (b) islanding control, (c-d) N-GI PLL and (e) N-GI structure
- Fig. 6.8 Control scheme of PVI-2
- Fig. 6.9 (a) PLL and (b) mode transition control
- Fig. 6.10 Simulation Model of a single stage multiple parallel PV inverter based microgrid
- Fig. 6.11 Simulation Model of a multiple parallel PV inverter based microgrid
- Fig. 6.12 Developed hardware phototype of multiple parallel PV inverter based microgrids
- Fig. 6.13 Performance of single stage system in solar insolation variation
- Fig. 6.14 Automatic mode transition performance from GIM to IAM and IAM to GTM in parallel operated PVI microgrid
- Fig. 6.15 Performance analysis of designed controller in GTM with varying PV insolation
- Fig. 6.16 Performance analysis of the designed controller in GTM with varying load demand
- Fig. 6.17 Harmonic pattern of (a)  $v_g$ , (b)  $v_{LI}$ , (c) unit-1 output current ( $i_{o1}$ ), (d) unit-2 output current ( $i_{o2}$ ) and grid current ( $i_g$ )
- Fig. 6.18 Mode transition of parallel PVIs while transferring from GTM to IAM and vice-versa
- Fig. 6.19 Performance of the microgrid in varying load condition
- Fig. 6.20 Performance of the two-stage parallel PVI-based microgrid under the load change.
- Fig. 6.21 Harmonic pattern of (a)  $v_g$ , (b)  $v_{LI}$ , (c) unit-1 output current ( $i_{o1}$ ), (d) unit-2 output current ( $i_{o2}$ ) and grid current ( $i_g$ )
- Fig. 6.22 Mode transition of parallel PVIs while transferring from GTM to IAM and vice-versa
- Fig. 6.23 Performance of the two-stage parallel PVI-based microgrid under the load change in IAM
- Fig. 7.1 Multiple parallel PV inverter-based microgrid with bidirectional buck-boost converter-controlled BES
- Fig. 7.2 Multiple parallel PV inverter-based microgrid with BES on DC link
- Fig. 7.3 Configuration of multiple parallel solar PV-BES inverter-based microgrids

- Fig. 7.4 Control strategy of PVI-1
- Fig. 7.5 Control scheme of PVI-2
- Fig. 7.6 Structure of ITOAI-QSG
- Fig. 7.7 Pole–Zero plot of ITOAI-QSG
- Fig. 7.8 (a) PLL and (b) mode transition control (MTC)
- Fig. 7.9 Adaptive control structure of main PVI-1 in single stage microgrid
- Fig. 7.10 Adaptive power control (APC) scheme of ancillary PVI-2
- Fig. 7.11 Structure of enhanced adaptive integrator
- Fig. 7.12 Pole-zero maps of EAI with different  $\xi$  values. (a) pole-zero maps of  $H_d(s)$ . (b) pole-zero maps of  $H_q(s)$
- Fig. 7.13 Control for transition between grid-connected and islanded mode
- Fig. 7.14 Control structure of main PVI-1 in two stage microgrid
- Fig. 7.15 Control scheme of ancillary PVI-2
- Fig. 7.16 Bode phase plot of AIF
- Fig. 7.17 Mode transition control logic
- Fig. 7.18 Simulation model of single-phase single-stage multiple parallel PV inverter based microgrid with bidirectional buck-boost converter-controlled BES
- Fig. 7.19 Simulation Model of a single-phase single stage multiple parallel PV inverter based microgrid with bidirectional buck-boost converter-controlled BES
- Fig. 7.20 Simulation Model of a single-phase two-stage multiple parallel PV inverter based microgrid with bidirectional buck-boost converter-controlled BES
- Fig. 7.21 Developed hardware phototype of multiple parallel PV inverter based microgrids.
- Fig. 7.22 Automatic mode transition performance from GIM to IAM and IAM to GTM in parallel operated PVI microgrid
- Fig 7.23 Harmonic spectra of (a) grid voltage, (b) grid current and (c) PCC voltage
- Fig 7.24 Performance analysis of designed controller in GTM with varying load demand
- Fig 7.25 Harmonic pattern of (a)  $i_g$ , (b)  $v_g$ , and (c)  $v_{LI}$
- Fig. 7.26 Performance analysis of designed controller in GTM with varying PV insolation
- Fig. 7.27 Seamless mode transition of parallel PVIs while transferring from GTM to IAM and vice-versa.
- Fig. 7.28 Simulated performance of residential PV system under automated mode transition
- Fig. 7.29 Harmonic spectra of (a-b) grid current ( $i_g$ ), (c-d) grid voltage ( $v_g$ ) and (e-f) PCC voltage ( $v_{LI}$ )

- Fig. 7.30 Performance of the microgrid in varying load condition (a) signals of PVI unit-1, (b-c) signals of PVI unit-2, (d-e) captured power signals.
- Fig. 7.31 Harmonic pattern (a)  $i_g$ , (b)  $v_g$ , and (c)  $v_{LI}$
- Fig. 7.32 Test performance of system with varying solar irradiation
- Fig. 7.33 Performance of the residential PV system under automated mode transition
- Fig. 7.34 Performance of microgrid in GTM under the load dynamic (a) system waveform, (b) power waveform, (c-d) harmonics spectrum
- Fig. 7.35 Performance of microgrid in GTM under mode transition (a) system waveform, (b) power waveform, (c-d) harmonics spectrum
- Fig. 7.36 Performance of microgrid in IAM under mode transition (a) system waveform, (b) power waveform, (c-d) harmonics spectrum
- Fig. 7.37 Performance of the two-stage parallel PVI based microgrid under the load change.
- Fig. 7.38 Performance of microgrid under varying solar insolation
- Fig. 7.39 Performance of microgrid under mode transition

## LIST OF TABLES

Table 2.1	List of IEEE/IET standards
Table 2.2	Grid Disconnection Time for Frequency Variation
Table 2.3	Reconnection of Grid Standard
Table 3.1	Details of the PV Array Simulator
Table 3.2	DSP Microcontroller Specifications
Table 3.3	Simulation Parameters of Single Stage PV-BES microgrid
Table 3.4	Experimental Parameters of Single Stage PV-BES microgrid
Table 3.5	Simulation Parameters of Two Stage PV-BES microgrid
Table 3.6	Experimental Parameters of Two Stage PV-BES microgrid
Table 3.7	Simulation Parameters of Two Stage PV-BES microgrid
Table 3.8	Experimental Parameters of Two Stage PV-BES microgrid
Table 4.1	Design Parameters of Grid Connected Wind-BES-based Microgrid
Table 4.2	Parameters of Wind Turbine
Table 4.3	Simulation Parameters of Two Stage Wind-Based AC Microgrid
Table 4.4	Hardware Parameters of Two Stage Wind-Based AC Microgrid
Table 4.5	Simulation Parameters of Single Phase Two Stage Wind Microgrid
Table 4.6	Hardware Parameters of Single Phase Two Stage Wind Microgrid
Table 5.1	Design Parameters of solar-wind-BES based Microgrid
Table 5.2	Design Parameters of solar-wind-BES based Microgrid with DBC
Table 5.3	Standard Range of Grid Parameters
Table 5.4	Simulation Parameters of Single-Phase Single Stage PV Wind and BES Microgrid
Table 5.5	Hardware Parameters of Single stage PV wind and BES microgrid Simulation Parameters of Single stage PV wind and BES microgrid
Table 5.7	Hardware Parameters of Single stage PV wind and BES microgrid Simulation Parameters of Single-Phase PV wind and BES microgrid
Table 5.9	Hardware Parameters of Single-Phase PV wind and BES microgrid
Table 6.1	Design Parameters of Single-Phase Grid Interactive Multiple Microgrid
Table 6.2	Design Parameters of Single-Phase Grid Interactive Multiple Microgrid
Table 7.1	Design Parameters of Single-Phase Grid Interactive Multiple Microgrid
Table 7.2	Design Parameters of single-Phase grid Interactive Multiple Microgrid

## LIST OF ABBREVIATIONS

ADO	Adaptive Disturbance Observer
AIF	Adaptive Integrator Filter
ANI	Active Noise Isolation
APF	Active power Filter
APC	Adaptive Power Control
AQSG	Adaptive Quadrature Signal Generator
BES	Battery Energy Storage
BPF	Band Pass Filter
CCM	Current Control Mode
DBC	DC-DC Bidirectional Converter
DOD	Depth of discharge
DSP	Digital Signal Processor
DER	Distributed Energy Resource
DFIG	Double-Fed Induction Generator
DFT	Discrete Fourier transformation
ES-SOGI	Extant State Second Order Generalized Integrator
FADO	frequency adaptive disturbance observer
FLL	Frequency Locked Loop
FSFP	Fixed Speed Fixed Pitch
FSVP	Fixed Speed Variable Pitch
GF-EPLL	General Filtering based Enhanced Phase Locked Loop
GI	Generalized Integrator
GTM	Grid Tied Mode
HE	Harmonic Extractor
HSC	Hysteresis Switching Controller
HVCC	Hybrid Voltage and Current Control
IAM	Islanding Mode
IGBT	Insulated Gate Bipolar Transistor
InC	Incremental Conductance
ITOAI	Improved Third-Order Adaptive Integrator
LMF	Least Mean Fourth

LMS	Least Mean Square
MACNE	Multi Adaptive Circular Noise Estimation
MNSOGI	Modified Novel Second Order Generalized Integrator
MCVF	Modified Complex Variable Filter
MOGI	Mixed Order Generalized Integrator
MPP	Maximum Power Point
MPE	Maximum Power Extraction
MADO	Multi Adaptive Disturbance Observer
NDZ	Non-Detection Zones
PCC	Point of Common coupling
PMBLDCG	Permanent Magnet Brushless DC Synchronous Generator
P&O	Perturb and observe
PI	Proportional Integral
PLL	Phase Locked Loop
PQ	Power Quality
PV	Photovoltaic
PVI	Photovoltaic Inverter
QSG	Quadrature Signal Generator
RTDS	Real Time Digital Simulator
RES	Renewable Energy Source
SOC	State of Charge
S&H	Sample and Hold
SOGI	Second Order Generalized Integrator
SOGI-QSG	Second Order Generalized Integrator with Quadrature Signal Generator
SRFT	Synchronous Reference Frame Theory
STS	Static Transition Switch
THD	Total Harmonic Distortion
TF	Transfer Function
TOGI	Third Order Generalized Integrator
TSP	Tip Speed Ratio
UPF	Unity Power Factor
UPS	Uninterruptible Power Supply

VCM	Voltage Control Mode
VSVP	Variable Speed Variable Pitch
VSC	Voltage Source Converter
VSFP	Variable Speed Fixed Pitch
WEGS	Wind Energy Generation System
WT	Wind Turbine
ZCD	Zero Crossing Detector

## LIST OF SYMBOLS

$a$	Overloading factor
$\beta$	Blade pitch angle
$A_g$	Battery ageing factor
$C_p^{\text{opt}}$	optimum power coefficient
$C_{dc}$	DC link capacitor
$C_p$	power coefficient
$C_f$	Ripple filter capacitance
$D$	Duty cycle of the bidirectional converter
$D_{bs}$	Duty cycle of the boost converter
$\Delta I_g$	Ripple in the grid current
$\Delta I_b$	Minimum ripple in the battery
$\Delta P_w$	Change in wind power
$\Delta I_{WT}$	Change in wind turbine current
$\Delta V_{WT}$	Change in wind turbine voltage
$\Delta P_{PV}$	Change in PV power
$\Delta V_{PV}$	Ripple in the PV voltage,
$\Delta I_{PV}$	Ripple in the PV current,
$\Delta \theta$	Phase angle error between the phase angle of grid and load voltage
$f_g$	Grid Frequency
$f_{g\text{min}}, f_{g\text{max}}$	Minimum and maximum AC side frequency
$G$	Solar Insolation
$I_{MP}$	Maximum PV Current
$I_{IGBT}$	Current rating of IGBT devices
$I_{dc}$	DC link current
$I_{PV}$	PV Current
$I_{sc}$	Short circuit current
$I_{wT}$	Rectifier wind current
$i_{wa}$	Stator phase 'a' current
$I_{VSC\text{max}}$	Maximum VSC current
$I_b$	Battery current
$I_b^*$	Reference battery current

$i_c$	VSC current
$I_{vd}, I_{vq}$	VSC current in DQ frame
$i_{s\alpha}, i_{s\beta}$	Reference grid current in $\alpha\beta$ -reference frame
$i_L$	Load currents
$i_{\alpha L}, i_{\beta L}$	Load current in $\alpha\beta$ -reference frame
$i_{\alpha Ls}, i_{\beta Ls}$	Reference load current in $\alpha\beta$ -reference frame
$I_{drg}, I_{drg}$	Reference grid current in DC frame
$I_{ld}, I_{Lq}$	Reference load current in DC frame
$I_{PVFF}$	PV Feedforward term
$I_{WTFF}$	Wind Feedforward term
$I_{Loss}$	DC loss component
$I_{pL}$	Active fundamental component of load current
$I_{gr}$	Net reference grid current
$i_{gref}$	Reference grid current
$J$	Equivalent moment of inertia
$K$	Derating Factor
$K_0, K_1, K_2$ and $K_3$	Internal gain parameters in GL-EPLL
$L_{bc}$	Boost converter inductor
$L_b$	bidirectional converter inductor
$L_f$	Interfacing Inductor
$m$	Modulation Index
$N_{P\_PV}$	Number of parallel solar PV panels
$N_{S\_PV}$	Number of series solar PV panels
$P_{PV}$	PV power
$P_L$	VSC power
$P_g$	Grid power
$P_{cgr}$	Constant grid power
$P_W$	Wind power
$R_f$	Ripple filter Resistance
$R_b$	Turbine blade radius
$S_{STS}$	Synchronization signal
$S_{vf}$	Safety factor for calculating voltage rating of IGBT devices

$S_{if}$	Safety factor for calculating current rating of IGBT devices
$T_c$	Temperature correction factor
$T$	Solar temperature
$V_{dcm}$	Minimum DC link voltage
$u_{pg}, u_{pq}$	In-phase and quadrature phase unit templates
$V_{IGBT}$	Voltage rating of IGBT devices
$V_{dc}$	DC link voltage
$V_{PV}$	PV voltage
$V_{oc}$	Open circuit voltage
$V_{dcr}$	Reference DC link voltage
$v_g$	Grid voltage
$v_{\alpha g}, v_{\beta g}$	Grid voltage in $\alpha\beta$ -reference frame
$V_d, V_q$	Grid voltage in DQ frame
$V_t$	Magnitude of grid voltage
$V_{tmin}, V_{tmax}$	Minimum and maximum AC grid voltage
$v_L$	Load voltage
$V_{Ld}, V_{Lq}$	Load voltage in $\alpha\beta$ -reference frame
$V_{ld}^*, V_{lq}^*$	Reference load voltage in $\alpha\beta$ -reference frame
$V_t$	Terminal voltage
$v_{wT}$	Rectifier wind voltage
$v_{wa}$	Stator phase 'a' voltage
$\omega_o$	Nominal value of grid frequency
$\omega$	grid frequency
$X_g$	Grid status signal
$\theta_L$	Phase angle of grid voltage
$\theta_g$	Phase angle of load voltage
$\lambda_{opt}$	Tip speed ratio